

Cite this: *Biomater. Sci.*, 2021, **9**, 4880

## A flexible microfluidic strategy to generate grooved microfibers for guiding cell alignment†

Mengqian Zhao,<sup>a,b</sup> Haitao Liu,<sup>a,b</sup> Xu Zhang,<sup>a</sup> Hui Wang,<sup>a,b</sup> Tingting Tao<sup>a,b</sup> and Jianhua Qin  <sup>a,b,c,d</sup>\*

Hydrogel microfibers are widely applied in tissue engineering and regenerative medicine due to their tunable morphology, componential anisotropy, and good biocompatibility. Specifically, grooved microfibers with unique advantages can facilitate cell alignment for mimicking the microstructures of myobundles. Herein, a microfluidic spinning system is proposed for flexibly generating grooved microfibers relying on the volume change after ionic crosslinking of sodium alginate (NaA) with different concentrations. In the system, multiple parallel channels are integrated into a flow-focusing microchip and NaA with various concentrations is introduced into the respective channels for fabricating well-defined microfibers. The size and shape of the fibers are tuned by the viscosity and concentration of the NaA solution, as well as the flow rates of NaA and calcium chloride (CaCl<sub>2</sub>) in a controllable manner. Moreover, the grooved fibers with heterogeneous components can be generated *via* co-spinning gelatin methacrylate (GelMA) and NaA to form interpenetrating polymer networks (IPNs). The microfibers with heterogeneous IPNs are successfully used as anisotropic scaffolds for the 3D culture of muscle cells (C2C12). The muscle cells grown on the microfibers exhibited good viability and ordered alignment, indicating the good biocompatibility and orientational function of the heterogeneous fibers. The proposed approach is flexible and controllable, holding potential in replicating various aligned microstructures *in vivo*, such as bundles of nerves and blood vessels.

Received 7th April 2021.

Accepted 3rd June 2021

DOI: 10.1039/d1bm00549a

rsc.li/biomaterials-science

### 1. Introduction

Recently, hydrogel microfibers have been emerging as promising scaffolds in materials science and tissue engineering due to their apparent advantages of high biocompatibility, tunable physicochemical properties, and unique fiber-shaped structures. These microfibers supply various biomimetic microenvironments, including gradient stiffness, cell-matrix interactions, and defined patterns, which facilitate cell growth, arrangement, migration, and differentiation.<sup>1–8</sup> To date, several methods are available to fabricate hydrogel microfibers, including electrospinning,<sup>9–11</sup> wet spinning,<sup>12,13</sup> self-assembly,<sup>14,15</sup> and microfluidic spinning.<sup>16–20</sup> Among these methods, the microfluidic spinning technology is widely used

for generating microfibers with designed structures or components due to the precise control of liquid flow and the property of laminar flow at the micro-scale. Different physical and chemical crosslinking methods can be applied in microfluidic spinning, such as solvent extraction, ionic crosslinking, and photopolymerization, permitting flexible selection of materials in such systems.<sup>16,18,21–24</sup> Furthermore, the microfluidic spinning method is derived from the microfluidic technique that could provide devices with multi-channels of different heights for flexibly manipulating multi-phase flows. Based on these features, microfibers with various structures (*e.g.*, hollow, tubular, porous, flat, and grooved) can be generated, which have the potential to rebuild blood vessels, bronchi, and neural bundles *in vitro*, as well as deliver cytokines or drugs.<sup>25–28</sup> Specifically, microfibers with multi-grooved structures exhibit unique advantages for constructing biomimetically aligned microstructures to facilitate the spreading, alignment, and differentiation of cells.<sup>10,29–32</sup>

In the last decade, many studies have been reported to establish microfluidic spinning methods to fabricate grooved microfibers based on the intrinsic design of microchannel size and nozzle geometry or using a rotary receiving pool.<sup>33–35</sup> Of these two methods, the former is limited by a fixed spinneret with a groove shape that determines the morphology of the

<sup>a</sup>CAS Key Laboratory of SSAC, Dalian Institute of Chemical Physics, Chinese Academy of Sciences, Dalian, 116023, P.R. China. E-mail: jhqin@dicp.ac.cn

<sup>b</sup>University of Chinese Academy of Sciences, Beijing, 100049, P.R. China

<sup>c</sup>Institute for Stem Cell and Regeneration, Chinese Academy of Sciences, Beijing, 100101, P.R. China

<sup>d</sup>CAS Center for Excellence in Brain Science and Intelligence Technology, Chinese Academy of Sciences, Shanghai, 200031, China

†Electronic supplementary information (ESI) available. See DOI: 10.1039/d1bm00549a

microfibers. When the prepolymer is sprayed out, it will cross-link and solidify quickly to maintain the shape of the grooved structure induced by the spinneret. As for the rotary receiving method, the prepolymer is extruded from the circular spinneret and then rotated for collection in the solution before curing to form grooved fibers. The limitation of this method is that the structure of grooved microfibers only depends on the design of the spinneret, which is less flexible. Furthermore, it is difficult for both methods to fabricate microfibers with heterogeneous components, which is one of the important factors for mimicking the cellular microenvironment. Therefore, a flexible and controllable strategy to generate grooved microfibers with defined structures and heterogeneous components is highly desired in this field.

In this work, we present a novel strategy for the fabrication of grooved microfibers that act as anisotropic scaffolds for muscle cell culture in the microfluidic spinning system. The generation of grooved microfibers relies on the *in situ* gelling of high and low concentrations of NaA, which results in a volume difference within the fibers after solidification. The morphology and size of the grooved fibers can be flexibly modulated by changing the concentration of NaA and the flow rates of samples in each channel. Simultaneously injecting different samples into the multi-parallel microchannels enables the preparation of heterogeneous grooved microfibers. Based on this method, microfibers with hydrogel IPNs can be successfully fabricated by the double crosslinking process of GelMA and NaA. In addition, the heterogeneous microfibers are preliminarily used as anisotropic scaffolds for muscle cell culture, which can guide the alignment and elongation of these cells, indicating the potential of such fibers to promote the maturity of muscle. The proposed approach exhibits the advantages of simplicity, flexibility, and controllability and has potential applications in materials science, regenerative medicine, tissue engineering, *etc.*

## 2. Materials and methods

### 2.1. Materials

SU-8 (3035) was purchased from Microchem. Sodium alginate ( $M_w = 50\ 000$ , NaA-LMW;  $M_w = 250\ 000$ , NaA-HMW) was purchased from Qingdao Hyzlin Biology Development Co. Anhydrous calcium chloride ( $\text{CaCl}_2$ ) and sodium chloride (NaCl) were purchased from Tianjin Damao Chemical Reagents Factory. Gelatin (Type A, 300 bloom from porcine skin) was purchased from Sigma-Aldrich. Methacrylic anhydride (MA) was purchased from Aladdin. 2-Hydroxy-4'-(2-hydroxyethoxy)-2-methylpropiophenone (Irgacure 2959) was purchased from TCI. A dialysis tube (12–14 kDa cut-off) was purchased from Yuanye Bio-Technology. All reagents were used as received.

### 2.2. Microfluidic device design and fabrication

The microfluidic device consisted of three layers, which are assembled using polydimethylsiloxane (PDMS) *via* soft litho-

graphy.<sup>28</sup> The top layer was the “inlet layer”, which contains 3 inlets for NaA-LMW, NaA-HMW and  $\text{CaCl}_2$  solutions. The middle and bottom layers with the same and symmetrical microchannels were bonded through oxygen plasma to form the “channel layer”. Then the “channel layer” was bonded with the “inlet layer” according to the position of the inlets. The height and width of the microchannels in the “channel layer” are as follows: the height and width of each dispersing channel are 100  $\mu\text{m}$  and 20  $\mu\text{m}$ . The height and width of the  $\text{CaCl}_2$  channel are 200  $\mu\text{m}$  and 400  $\mu\text{m}$ . The height and width of the laminar flow channel are 200  $\mu\text{m}$  and 1400  $\mu\text{m}$ . The height and width of the solidification channel are 200  $\mu\text{m}$  and 2600  $\mu\text{m}$ .

### 2.3. Preparation of CaA microspheres

NaA solutions were prepared with different concentrations (NaA-LMW: 1%, 2%, 3% and 4% (w/v); NaA-HMW: 0.5%, 1%, 1.5% and 2% (w/v)) in water. Microspheres were prepared by the hanging drop method. NaA solutions were ejected at a flow rate of 0.2  $\text{mL min}^{-1}$  by using a syringe pump. The volume of each droplet is 30  $\mu\text{L}$ . The droplets of NaA were dropped into a beaker containing 2% (w/v)  $\text{CaCl}_2$  solution directly. Then the microspheres were immediately moved from the beaker. The excess water on the hydrogel microspheres was removed with weighing paper. The diameter of the microspheres was measured using ImageJ based on the bright field images.

### 2.4. Viscosity measurement

The viscosities of NaA solutions with different concentrations were measured using a rotational viscometer (NDJ-5S, Shanghai Changji Geological Instrument Co. Ltd., China) at room temperature. The spindle of the viscometer was rotated within the sample tubes at a constant speed of 20 rpm.

### 2.5. GelMA synthesis

GelMA was synthesized using our previous protocol.<sup>36</sup> Briefly, 5 g of gelatin was dissolved in 50 mL of Dulbecco's phosphate-buffered saline (DPBS, Invitrogen) at 60 °C. Then, 4 mL of MA was added into the above solution at a rate of 0.5  $\text{mL min}^{-1}$  for 1 h under stirring at 50 °C. The reaction was stopped by adding 250 mL of DPBS of 40 °C. The mixture was dialyzed at 40 °C for 1 week using a cut-off tube (12–14 kDa). The solution was lyophilized for 1 week and stored at –80 °C until further use.

### 2.6. Controlled preparation of hydrogel microfibers

NaA solution was sterilized *via* a filter (0.22  $\mu\text{m}$  membrane). To generate grooved fibers, the following solutions were introduced into the microfluidic device: (1) NaA solution with a high concentration ( $\text{NaA}_{(\text{H})}$ ) was injected into inlet 1 to generate the convex areas of the fiber; (2) NaA solution with a low concentration ( $\text{NaA}_{(\text{L})}$ ) was injected into inlet 2 to form the concave areas of the fiber; and (3) 2% (w/v)  $\text{CaCl}_2$  solution was injected into inlet 3 as sheath flow to solidify the fiber. The flow rates of NaA within each parallel channel ranged from 0.5  $\mu\text{L min}^{-1}$  to 2.5  $\mu\text{L min}^{-1}$ , and the flow rates of  $\text{CaCl}_2$

ranged from  $3000 \mu\text{L min}^{-1}$  to  $5000 \mu\text{L min}^{-1}$ . GelMA with a concentration of 5% (w/v) was added to the system to generate homogeneous GelMA–CaA microfibers under the aforementioned conditions. After ionic crosslinking within the channels, the microfibers were exposed to UV light (365 nm, intensity 8 mW) for 3 min in a solution containing 0.25% (w/v) Irigacure 2959 and 2% (w/v)  $\text{CaCl}_2$  for secondary crosslinking. To generate microfibers with heterogeneous components, a solution of 3.4% (w/v) NaA-HMW was introduced into inlet 1. The other solutions were the same as those used for the generation of homogeneous GelMA–CaA microfibers.

### 2.7. Scanning electron microscopy (SEM)

To observe the surface morphology, the microfibers were cut into short pieces (about 1–2 mm) after being washed with ultrapure water 3 times. Then the microfibers were dehydrated with gradient ethanol (25, 50, 75 and 100%; 10 min each) and then placed in an 80 °C oven overnight. After metal spraying, the fibers were characterized using a scanning electron microscope (SEM, Hitachi TM3000, Japan) at 15 kV. The microfiber seeded cells were fixed with 2.5% glutaraldehyde for 1 h and gently washed 3–5 times with deionized water. Then, the samples were dehydrated with a series of graded ethanol solutions in the same way. After dehydration, the samples were immersed in *tert*-butyl alcohol for 30 min (two times) at room temperature and frozen at –80 °C. Finally, the samples were freeze-dried in a lyophilizer for 3 days and the SEM images were obtained.

### 2.8. Cell culture

Murine skeletal myoblasts (C2C12) were purchased from the China Center for Type Culture Collection. They were cultured in Dulbecco's modified Eagle's medium (DMEM, high glucose, Gibco) that was supplemented with 1% streptomycin–penicillin (Beyotime) and 10% fetal bovine serum (FBS, Gibco). The C2C12 cells were maintained in an incubator with 5%  $\text{CO}_2$  at 37 °C, and the medium was changed every 2 days.

### 2.9. Cell seeding on the microfibers

Before cell seeding, the GelMA–NaA hybrid microfibers were rinsed with DPBS to remove the residual photoinitiator. Then the microfibers were wrapped around PDMS plates in a **6-well culture plate (Guangzhou Jet Bio-Filtration Co., Ltd.)** and sterilized by UV irradiation overnight. At 60–70% confluence, C2C12 cells were harvested by using 0.25% trypsin–EDTA (Gibco) and seeded on grooved fibers ( $5 \times 10^6$  cells per mL). After the microfibers were cultured in an incubator for 2 h to allow cell attachment, the warm growth medium (2 mL) was added into the dish.

### 2.10. Cell viability analysis

The viability of C2C12 cells on the microfibers was evaluated using a Live/Dead Cell Viability Kit (BD) according to the manufacturer's staining protocol.<sup>37</sup> Cell-laden microfibers were washed with physiological saline 3 times. Then, the microfi-

bers were incubated in live/dead staining reagents for 30 min at 37 °C.

### 2.11. Immunofluorescence of C2C12 fibroblasts

Cell-laden microfibers were gently rinsed with physiological saline and fixed with 4% paraformaldehyde (Tianjin Damao Chemical Reagents Factory) for 30 min. Then, the samples were permeabilized with 1% Triton X-100 (MeilunBio) in physiological saline for 15 min. Finally, the samples were stained with Phalloidin Conjugate reagents (Biotium) and 4',6-diamidino-2-phenylindole dihydrochloride (DAPI, Cell Signaling Technology) for 20 min. Images were acquired using an Olympus IX-71 inverted microscope (Olympus Corporation, Japan).

## 3. Results and discussion

### 3.1 Design and fabrication of the microfluidic device

To date, most of the existing hydrogel microfibers are cylindrical, lacking topographical features for recapitulating the structural complexity and functions of the native ECM within target tissues. Grooved microfibers utilize the topographical properties to align cells during cultivation. To generate grooved microfibers in a controllable and flexible manner, we designed and fabricated a microfluidic spinning device that consisted of three PDMS layers (Fig. S1†). As shown in Fig. 1A, the microchip contains three functional units: a diversion unit, a laminar flow unit and a solidification unit. The diversion unit was connected to the syringe pumps, which could evenly distribute sample A ( $\text{NaA}_{(\text{H})}$ , NaA with high concentration) into four separated microchannels and sample B ( $\text{NaA}_{(\text{L})}$ , NaA with low concentration) into three separated microchannels. Then, the above 7 microchannels were converged in the laminar flow unit that was a wide channel to enable samples A and B to generate parallel laminar flow (4 sample A areas and 3 sample B areas) with defined intervals. Finally, the laminar flow of NaA and the sheath flow ( $\text{CaCl}_2$  solution) went into the solidification unit together to form the coaxial flow and the NaA solution was solidified immediately in this step to form grooved fibers. The principle of generating grooved microfibers is shown in Fig. 1B. The solidification of the microfibers could be easily achieved through a rapid ionic-crosslinking reaction of NaA and  $\text{CaCl}_2$  without blocking the microchannel. This cross-linking between  $\text{Ca}^{2+}$  and alginate to form a gel is known as “the egg-box model”<sup>38</sup> (Fig. 1C). During the fiber spinning process, a laminar flow of NaA solutions with high and low concentrations was formed with defined intervals.  $\text{NaA}_{(\text{H})}$  would generate a high water content of CaA fibers after crosslinking to form a hydrogel with a larger volume, which was the convex part in the microfiber. Accordingly,  $\text{NaA}_{(\text{L})}$  would form a hydrogel with a lower volume, which appeared as the concave part in the microfiber. Furthermore, if we added different biochemical factors in flows A and B, microfibers with heterogeneous components could be formed. A PDMS microchip with three functional units was successfully fabri-

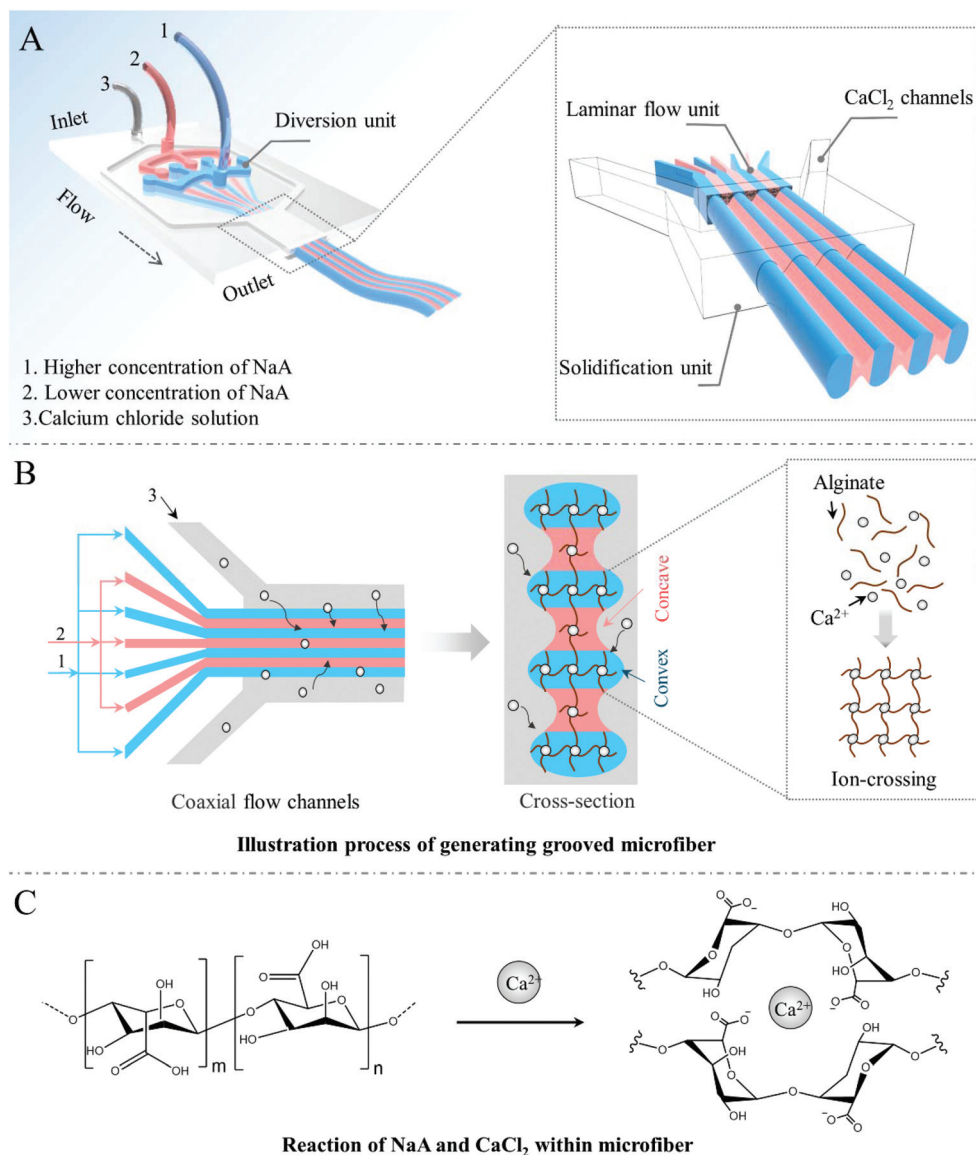


**Fig. 1** The schematic diagram of a microfluidic chip with multichannels for the preparation of grooved microfibers. (A) An overview of the system. Inlets 1–3 represent the inlets of sodium alginate with a high concentration, sodium alginate with a lower concentration, and calcium chloride solution, respectively. (B) Schematic diagram of the grooved microfibers generated at coaxial co-flow with different concentrations of sodium alginate. (C) A schematic illustration of the reaction process of NaA and CaCl<sub>2</sub> within the microfibers.

cated in this work, exhibiting good processing technology and well-designed microchannel structures. Compared with other devices for generating grooved fibers, this microchip provides the diversity of components in microfibers and also realizes precise control over the grooves of microfibers by separately changing each sample. In the proposed system, the complex extrusion channel and spinneret are avoidable, which simplifies the chip fabrication and fiber collection process.

### 3.2 Optimization of the parameters of the microfluidic system

To generate microfibers with consistent and controllable dimensions, several key parameters that might impact the morphology of grooved microfibers, such as the concentration

and viscosity of NaA solutions, the flow rate of CaCl<sub>2</sub>, and the ratio of rates in flows A and B, are systematically investigated in the system. Here, we measured the volume change of NaA solution after solidification, the total width of the microfibers ( $W_{\text{fiber}}$ ) and the groove width of the microfibers ( $W_{\text{groove}}$ ) under various conditions.

**3.2.1 Characterization of the NaA volume change after solidification.** To clarify the relationship between the concentration of the NaA solution and the size of the generated hydrogel, we used two types of NaA prepolymer (NaA-LMW ( $M_w = 50\,000$ ) and NaA-HMW ( $M_w = 250\,000$ )) with various solution concentrations to prepare microspheres using the hanging drop method (Fig. 2A). The volume of each NaA droplet was controlled *via* a syringe pump. The results revealed

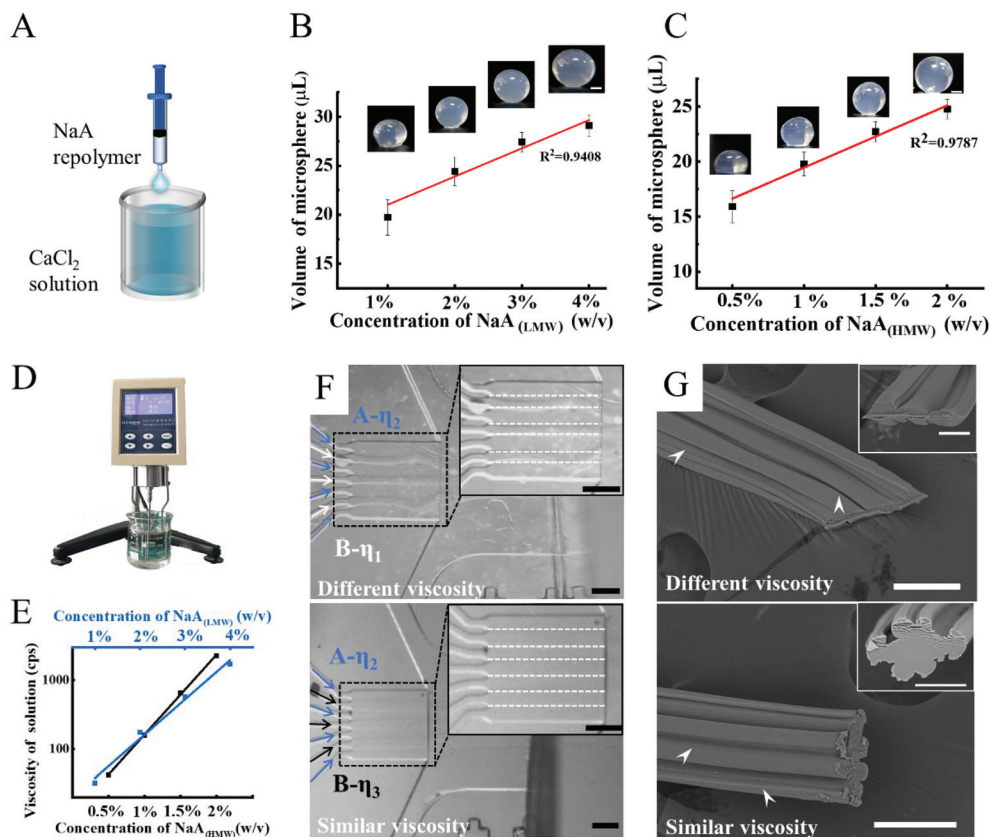


**Fig. 2** Effects of the viscosity and concentration of NaA on the morphology of the microfibers. (A) Schematic of the hanging drop method to fabricate microspheres. (B) Size of the microspheres as a function of the concentration of NaA with a low molecular weight (NaA<sub>(LMW)</sub>). The insets are bright-field images of microspheres generated with different concentrations of NaA<sub>(LMW)</sub> of 1%, 2%, 3% and 4%, respectively. Scale bar: 1 mm. (C) Size of microspheres as a function of the concentration of NaA with a high molecular weight (NaA<sub>(HMW)</sub>). The insets are bright-field images of microspheres generated with different concentrations of NaA<sub>(HMW)</sub> of 0.5%, 1%, 1.5% and 2%, respectively. Scale bar: 1 mm. (D) The schematic diagram of the viscosity measurement. (E) The viscosity as a function of the different concentrations and types of NaA. (F) Bright-field image of the laminar flow in the spinning orifice with different viscosities (top) and similar viscosities (bottom) of NaA. The insets show the enlarged images of the laminar flow. Scale bar: 500 μm. (G) SEM images of microfibers generated with different viscosities (top) and similar viscosities (bottom) of NaA. Scale bar: 100 μm. The insets show the SEM images of the cross sections of microfibers. Scale bar: 50 μm. The concave and convex parts are indicated by arrows.

that the concentration of NaA solution had a linearly positive correlation with the volume of the solidified microspheres (Fig. 2B and C). For the NaA-LMW, when the concentration increased from 1% to 4% (w/v), the volume of the microspheres increased from  $19.73 \pm 1.81 \mu\text{L}$  to  $29.09 \pm 1.05 \mu\text{L}$ ,  $R^2 = 0.9408$ . Similarly, when the concentration of NaA-HMW increased from 0.5% to 2% (w/v), the volume of the microspheres increased from  $15.91 \pm 1.43 \mu\text{L}$  to  $24.78 \pm 0.87 \mu\text{L}$ ,  $R^2 = 0.9787$ . This phenomenon is the experimental basis of this work to generate the groove structure on the microfibers. This phenomenon is caused by the fact that the hydrogel generated with a high NaA concentration could lock more water in the gel, while the hydrogel generated with a low NaA concentration would lose less water during solidification. Then, we measured the absolute water content (AWC) of the microspheres. For NaA-LMW, the AWC of the microspheres increased from  $20.78 \pm 0.21 \text{ mg}$  to  $27.56 \pm 0.55 \text{ mg}$  ( $R^2 = 0.9876$ ) when the concentration of NaA-HMW was increased from 1% to 4% (w/v)

(Fig. S2A†). Similarly, the AWC of the microspheres increased from  $17.76 \pm 0.27 \text{ mg}$  to  $25.13 \pm 0.42 \text{ mg}$  ( $R^2 = 0.9696$ ) when the concentration of NaA-HMW was increased from 0.5% to 2% (w/v) (Fig. S2B†). The results were consistent with our hypothesis.

**3.2.2 Effects of the NaA viscosity on the microfiber morphology.** In addition to the NaA concentration, the NaA viscosity was another factor that may affect the morphology of the grooved microfibers in our system. To demonstrate the effects of the NaA viscosity on the morphology of the microfibers, the microfibers generated using NaA with different viscosities were measured. The viscosity of the NaA solution depends on the concentration and molecular weight of NaA.<sup>39–41</sup> In this work, a rotational viscometer was used to measure the viscosity of the NaA solution (both NaA-HMW and NaA-LMW) with various concentrations. The results showed that the viscosity of the NaA solution increased exponentially with an increase of the NaA concentration, which was consistent

ent with the theory on the critical overlap concentration of the polymer solution.<sup>42,43</sup> As shown in Fig. 2E, the viscosity of 2% (w/v) NaA-LMW was similar to that of 1% (w/v) NaA-HMW, which provided the concentrations of alginate for reference in the following experiments.

To explore the importance of the viscosity on the morphology of the microfibers, we tested two conditions for generating the grooved microfibers: (1) generating the microfibers with both different concentrations and different viscosities of the NaA solutions and (2) using NaA solutions with different concentrations but similar viscosities for fabricating hydrogel fibers. To perform this, we chose sample A- $\eta$ 2 (2% NaA-LMW) and sample B- $\eta$ 1 (1% NaA-LMW) as examples of the former and chose sample A- $\eta$ 2 (2% NaA-LMW) and sample B- $\eta$ 3 (1% NaA-HMW) as examples of the latter in this testing. The results demonstrated that in condition 1 (different viscosity), the laminar flow of the interval NaA solution was disturbed, which resulted from the different surface tensions of the solutions with different viscosities. However, in condition 2 (similar viscosity), a stable laminar flow was observed in the microchannel (Fig. 2F). To further verify the results, we characterized the morphology of the microfibers by SEM (Fig. 2G). The results showed that the grooved morphology of the microfibers generated in condition 2 was more prominent and uniform than that in condition 1, indicating that similar viscosities of NaA solutions were more appropriate to fabricate grooved fibers in our system. This result was consistent with a previous study on fluid stability in a microchip.<sup>44</sup> Herein, we selected 2% NaA-LMW and 1% NaA-HMW for the following experiments in consideration of fluid stability and morphology controllability.

**3.2.3 Effects of the flow rates on the microfiber morphology.** Since the grooved microfibers are formed by multiple parallel laminar solutions, the proportion of each flow will directly affect the structure of the grooved microfibers. Therefore, we systematically studied the effects of the flow rates of the NaA solutions and CaCl<sub>2</sub> solution on the morphology of the microfibers. We defined the total width of the microfibers as  $W_{\text{fiber}}$  and the width of the groove within the microfibers as  $W_{\text{groove}}$  in the system (Fig. 3A). Also, grooved microfibers with red and green fluorescent bead dyes were investigated under a confocal laser scanning microscope (CLSM) (Fig. 3B). To intuitively observe the morphology of the microfibers within the microchip, NaA<sub>(H)</sub> and NaA<sub>(L)</sub> were mixed with blue and red dyes, respectively.

Firstly, we studied the effects of NaA<sub>(L)</sub> on the size of the microfibers. To perform this, the flow rates of CaCl<sub>2</sub> and NaA<sub>(H)</sub> were fixed to 4000  $\mu\text{L min}^{-1}$  and 1  $\mu\text{L min}^{-1}$  within each parallel channel, respectively. As shown in Fig. 3C, when the flow rate of NaA<sub>(L)</sub> was tuned from 0.5  $\mu\text{L min}^{-1}$  to 2.5  $\mu\text{L min}^{-1}$  within each parallel channel, the  $W_{\text{fiber}}$  increased from 356.81  $\pm$  7.82  $\mu\text{m}$  to 436.13  $\pm$  11.46  $\mu\text{m}$ , which was a linear fit to  $y = 39.41x + 335.08$ ,  $R^2 = 0.9797$ , while each  $W_{\text{groove}}$  increased from 35.26  $\pm$  2.17  $\mu\text{m}$  to 98.33  $\pm$  5.51  $\mu\text{m}$ , which was a linear fit to  $y = 31.27x + 19.14$ ,  $R^2 = 0.991$ . The proportion of the grooves in the total microfibers ( $3 \times W_{\text{groove}}/W_{\text{fiber}}$ ) was increased from

0.29 to 0.67, which was consistent with the proportion of the NaA<sub>(L)</sub> flow rate in the total flow rate of NaA<sub>(L+H)</sub> (Fig. 3D). This result demonstrated that the flow rate of NaA<sub>(L)</sub> would slightly influence the  $W_{\text{fiber}}$ , but significantly affect the morphology of the microfibers, especially the proportion of grooves in the total microfibers. The bright-field images of microfibers generated at different flow rates are shown in Fig. S3A,† which clearly displays the increase of the grooved area with an increase of the NaA<sub>(L)</sub> flow rate.

To evaluate the influence of NaA<sub>(H)</sub> on the size and morphology of the microfibers, the flow rate of NaA<sub>(H)</sub> was changed from 0.5  $\mu\text{L min}^{-1}$  to 2.5  $\mu\text{L min}^{-1}$ , while the flow rates of NaA<sub>(L)</sub> and CaCl<sub>2</sub> were fixed to 1  $\mu\text{L min}^{-1}$  and 4000  $\mu\text{L min}^{-1}$  in each channel, respectively. As shown in Fig. 3E, the  $W_{\text{fiber}}$  increased from 300.59  $\pm$  44.95  $\mu\text{m}$  to 426.30  $\pm$  12.08  $\mu\text{m}$  with an increase of the flow rate of NaA<sub>(H)</sub>, which was a linear fit to  $y = 38.62x + 338.15$ ,  $R^2 = 0.7252$ , while the  $W_{\text{groove}}$  decreased from 57.79  $\pm$  8.98  $\mu\text{m}$  to 30.83  $\pm$  1.55  $\mu\text{m}$ , which was a linear fit to  $y = -14.15x + 66.45$ ,  $R^2 = 0.9809$ . The proportion of grooves in the total microfibers ( $3 \times W_{\text{groove}}/W_{\text{fiber}}$ ) was decreased from 0.57 to 0.21, which was consistent with the proportion of the NaA<sub>(L)</sub> flow rate in the total flow rate of NaA<sub>(L+H)</sub> (Fig. 3F). We also studied the effects of the total flow rate of NaA on the size of the microfibers (Fig. S3B†). Herein, the flow rates of NaA<sub>(L)</sub> and NaA<sub>(H)</sub> were increased from 1.0  $\mu\text{L min}^{-1}$  to 3.0  $\mu\text{L min}^{-1}$  in each channel simultaneously. The result showed that both  $W_{\text{groove}}$  and  $W_{\text{fiber}}$  increased with an increase of the total flow rate of NaA, but the growth rates of  $W_{\text{groove}}$  and  $W_{\text{fiber}}$  (1.26 fold and 1.09 fold, respectively) were much lower than that of the total NaA flow rate (3.00 fold). Furthermore, the results also revealed that when the flow rates of NaA<sub>(L)</sub> and NaA<sub>(H)</sub> were changed simultaneously and equally, the proportion of grooves in the microfibers was almost unchanged (Fig. S3C†).

Finally, we explored the influence of the flow rate of the CaCl<sub>2</sub> solution on the microfibers. The flow rate of NaA within each parallel channel is 2  $\mu\text{L min}^{-1}$ , and the flow rate of CaCl<sub>2</sub> ranges from 3000 to 5000  $\mu\text{L min}^{-1}$ . The result showed that both the  $W_{\text{fiber}}$  and  $W_{\text{groove}}$  decreased with an increase of the CaCl<sub>2</sub> flow rate. The  $W_{\text{fiber}}$  was reduced from 437.22  $\pm$  7.36  $\mu\text{m}$  to 290.29  $\pm$  10.16  $\mu\text{m}$  and the  $W_{\text{groove}}$  was reduced from 61.82  $\pm$  2.98  $\mu\text{m}$  to 43.48  $\pm$  3.36  $\mu\text{m}$  (Fig. 3G). Moreover, the proportion of the grooves in the total fibers was unchanged during this process (Fig. 3H). Based on all the above results, we can conclude that (1) the flow rate of CaCl<sub>2</sub> solution only affects the  $W_{\text{fiber}}$  and the high flow rate of CaCl<sub>2</sub> will squeeze the NaA phase to reduce the  $W_{\text{fiber}}$ ; (2) the total flow rate of NaA<sub>(L+H)</sub> will affect the  $W_{\text{fiber}}$  as well. Oppositely, the increase of  $W_{\text{fiber}}$  is not in direct proportion to the flow rate of NaA, and the influence coefficient of the NaA flow rate on  $W_{\text{fiber}}$  is only 0.36 (1.09/3 = 0.36). This means that if the total NaA<sub>(L+H)</sub> flow rate increases 1-fold, the  $W_{\text{fiber}}$  only increases 0.36-fold, but the spinning speed will be faster; (3) the morphology of the grooved microfibers mainly depends on the ratio of the NaA<sub>(H)</sub> and NaA<sub>(L)</sub> flow rates. Since the viscosities of the NaA<sub>(H)</sub> and NaA<sub>(L)</sub> solutions are similar in this system, the NaA<sub>(H)</sub> pro-

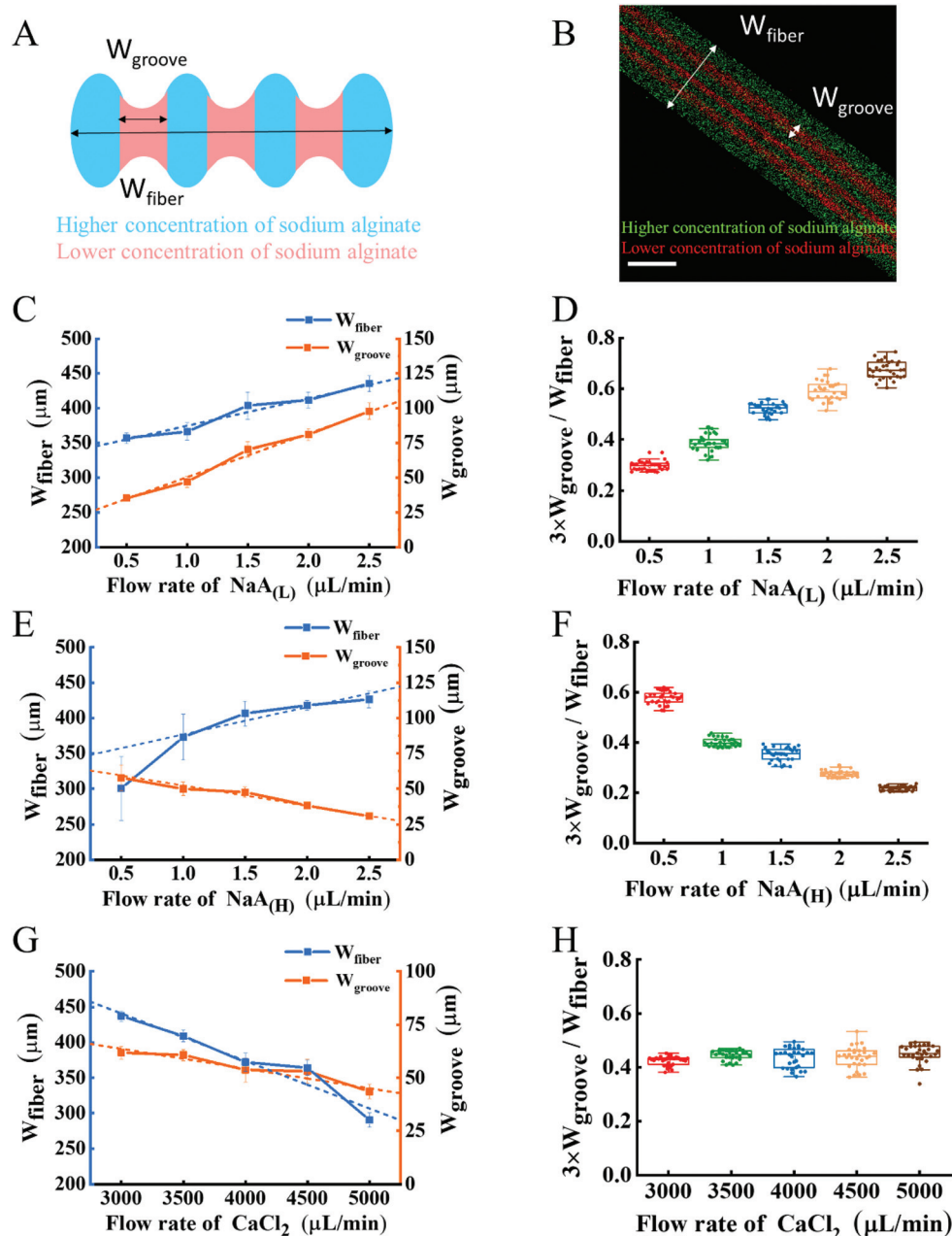


**Fig. 3** Effects of the flow rates on the morphology of microfibers. (A) The definitions of the width of microfibers ( $W_{fiber}$ ) and the width of the groove ( $W_{groove}$ ) within microfibers. (B) Confocal laser scanning microscopy (CLSM) image of grooved microfibers. (C) The effects of the flow rates of  $\text{NaA}_{(L)}$  on  $W_{fiber}$  and  $W_{groove}$ . (D) The effects of the flow rates of  $\text{NaA}_{(L)}$  on the proportion of grooves within microfibers ( $3 \times W_{groove}/W_{fiber}$ ). (E) The effects of the flow rates of  $\text{NaA}_{(H)}$  on  $W_{fiber}$  and  $W_{groove}$ . (F) The effects of the flow rates of  $\text{NaA}_{(H)}$  on the proportion of grooves within microfibers ( $3 \times W_{groove}/W_{fiber}$ ). (G) The effects of the  $\text{CaCl}_2$  flow rate on  $W_{fiber}$  and  $W_{groove}$ . (H) The effects of the  $\text{CaCl}_2$  flow rate on the proportion of grooves within microfibers ( $3 \times W_{groove}/W_{fiber}$ ). The concentrations of  $\text{NaA}_{(H)}$  and  $\text{NaA}_{(L)}$  are 2% and 1% NaA-HMW, respectively, for all.

portion determines the convex width and the  $\text{NaA}_{(L)}$  proportion determines the groove width.

### 3.3 Generation of heterogeneous microfibers

After optimizing the parameters of the microspinning system, we tried to fabricate grooved microfibers with heterogeneous components. NaA is one of the most widely used materials for making ultrafine fibers and 3D scaffolds because of its rapid

ionic gelation to form CaA. Gelatin methacrylate (GelMA) is a suitable material used as a bioscaffold due to its unique properties, such as good biocompatibility and biodegradability, and allowing cell adhesion and elongation on it.<sup>45–49</sup> In this work, we chose NaA and GelMA to generate heterogeneous microfibers with IPNs.

The schematic diagram of the IPN crosslinking process of NaA and GelMA is shown in Fig. 4A. Briefly, the IPN hydrogel

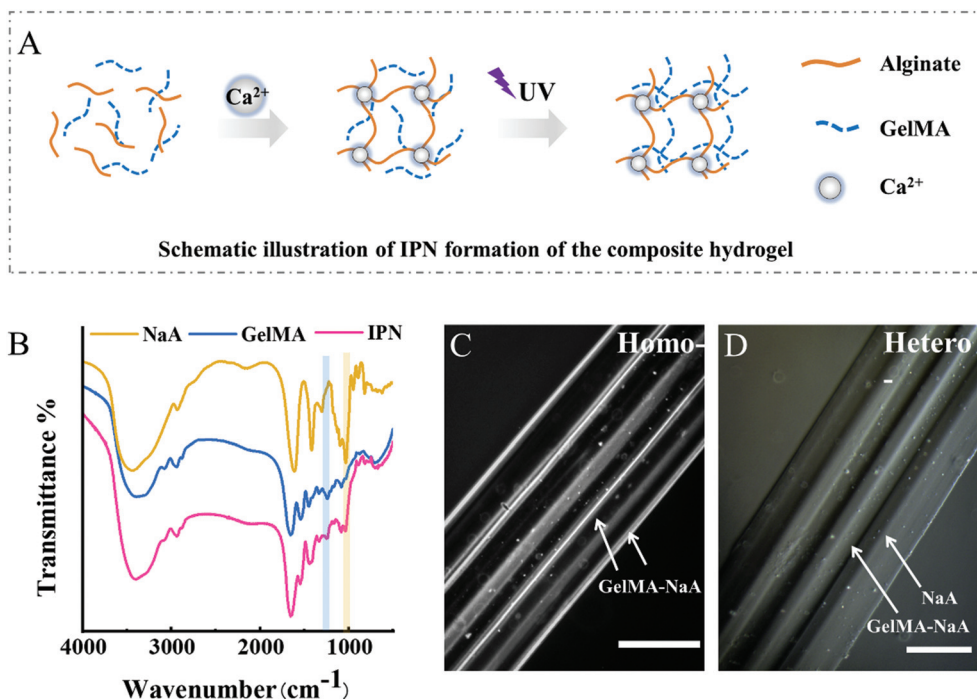


Fig. 4 The generation and characterization of the heterogeneous microfibers with interpenetrating polymer network (IPN) hydrogels. (A) Schematic illustration of IPN formation of the composite hydrogel. (B) Fourier transform infrared (FTIR) spectra of NaA and GelMA, and the IPN (NaA–GelMA) hydrogels. (C and D) Bright-field images of grooved homogeneous /heterogeneous fibers. Scale bar: 500  $\mu\text{m}$ .

of GelMA and CaA was formed *via* a two-step method composed of ionic crosslinking and photopolymerization reactions. To ensure consistency in the viscosity in this system, homogeneous fibers were generated with 5% GelMA–2% NaA-LMW and 5% GelMA–1% NaA-HMW and heterogeneous fibers were generated with 3.4% NaA-LMW and 5% GelMA–1% NaA-HMW. More detailed preparation conditions are described in the Materials and methods section. In order to prove the formation of the hybrid hydrogel, we characterized the surficial chemical groups of GelMA, CaA and GelMA–CaA hydrogel samples using Fourier transform infrared (FTIR) spectroscopy (Fig. 4B). The result demonstrated that the specific peak of CaA was at around 1030  $\text{cm}^{-1}$ , attributed to the stretching of C–O–C. The specific peak of GelMA was at 1590  $\text{cm}^{-1}$ , related to the N–H bending vibration and the C–N stretching vibration. The IPN hydrogel sample contains the characteristic peaks of both GelMA and CaA at 1030  $\text{cm}^{-1}$  and 1590  $\text{cm}^{-1}$ , which proved that the hybrid hydrogel of GelMA–CaA was successfully generated in this work. The bright-field images of homogeneous (GelMA–CaA) and heterogeneous (GelMA–CaA and CaA alone) microfibers are shown in Fig. 4C and D.

### 3.4 Grooved microfibers as anisotropic scaffolds for cell alignment

Skeletal muscle tissue has longitudinally aligned myofibrils that are formed by the fusion of myoblasts. Therefore, the alignment of myoblasts and their fusion is a prerequisite for

the reconstruction of the skeletal muscle tissue *in vitro*. Grooved microfibers have the topographical architecture needed to recapitulate the structural complexity and function of native tissues. The GelMA–NaA microfibers with grooved surfaces were fabricated allowing the culture of muscle cells on the microstructured surface to generate complex tissues. The C2C12 cells were seeded on the homogeneous (GelMA–CaA)/heterogeneous (GelMA–CaA and CaA alone) microfibers, respectively (Fig. 5A). Then the viability and orientation of the cells were investigated. As shown in Fig. 5B, the C2C12 cells could grow on both homogeneous and heterogeneous microfibers and the viability of the cells was good; the cell viabilities of C2C12 were 97.24% and 95.12%, respectively. Besides, based on the fluorescence images, we found that on homogeneous microfibers, the C2C12 cells grew on the whole surface of the fiber, including the grooves and convex part; however, on the heterogeneous microfibers, the cells only grew on the grooves of the fiber (Fig. 5C). The bright-field images and SEM images of the cells on the microfibers further confirmed this phenomenon (Fig. S4† and Fig. 5D). The results were attributed to the different bio-adherence values of GelMA and CaA hydrogels. Moreover, we can see that the C2C12 cells were more aligned and elongated on the heterogeneous microfibers in the SEM images, which could promote the maturity of the muscle.<sup>50</sup> The reason for this phenomenon was that the cells were more confined in the grooves.

To quantify the alignment and elongation of the cells on the microfibers, we further investigated the distribution of the

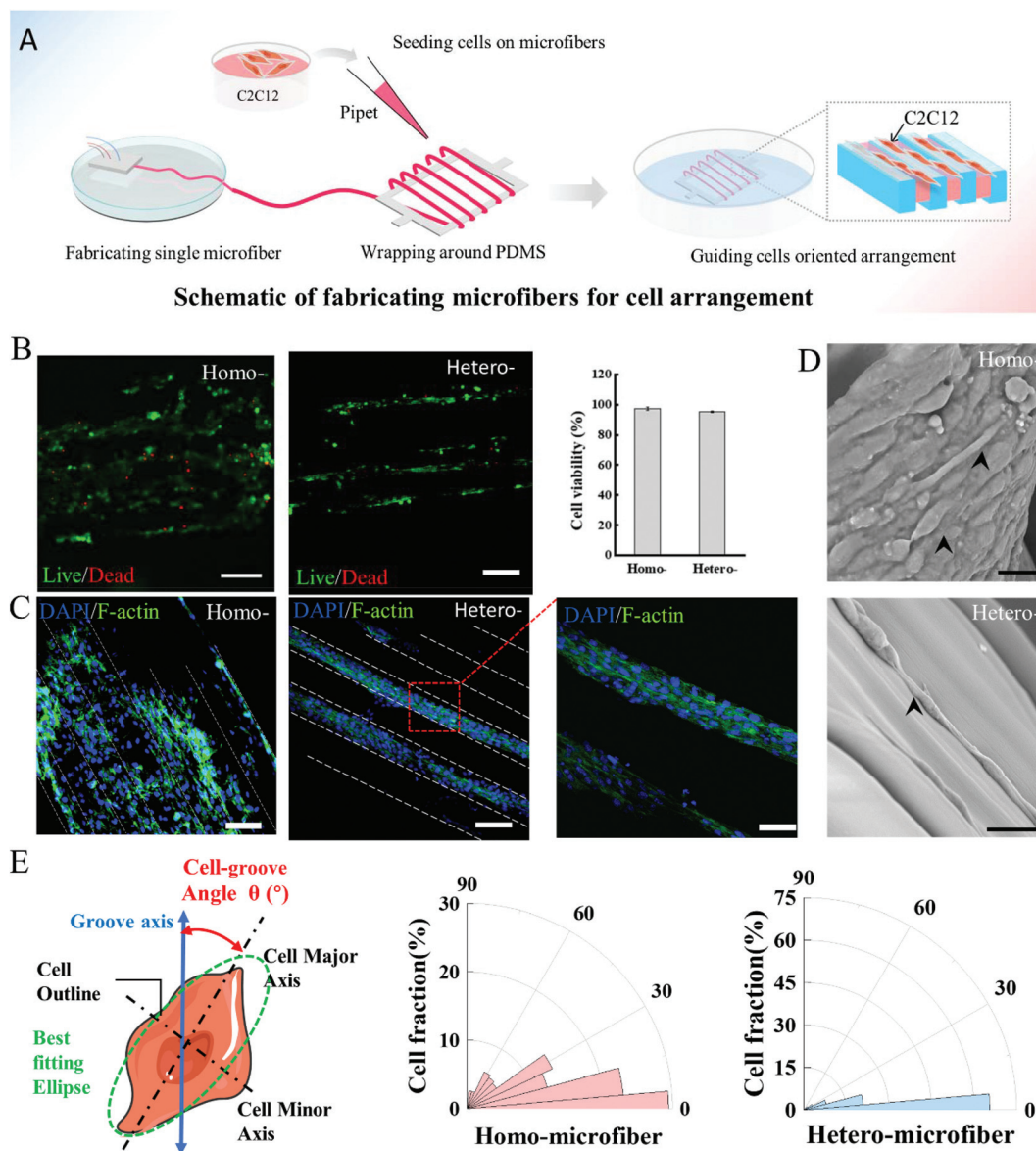


**Fig. 5** Cell alignments induced by the grooved microstructure on homogeneous/heterogeneous IPN hydrogel fibers. (A) The process of the microfibers utilized as anisotropic scaffolds for murine myoblast cell (C2C12) culture. (B) The live/dead fluorescence images of the cultured C2C12 cells on homo-(left) and hetero-(middle) grooved microfibers at day 3. Percentage viability of seeded cells on grooved microfibers (right). The results shown are mean values  $\pm$  s.d. ( $N = 3$ ). (C) Fluorescence images showing the orientation of F-actin (green) and cell nuclei (blue) within cells on homogeneous (left) and heterogeneous (middle and right) grooved microfibers. (D) SEM images showing cells on homogeneous (top) and heterogeneous (bottom) grooved microfibers. (E) The schematic showing  $\theta$  defined by an intersection angle between the major axis of cells and the micro-groove direction. Quantitative analysis of cell alignment on homogeneous (middle)/heterogeneous (right) grooved microfibers. Scale bar: 100  $\mu\text{m}$ .

direction (the angle between the major axis of the cell and the long axis of the basal fiber) of these cells (Fig. 5E). The results demonstrated that on the flat GelMA–CaA slab, the orientation of the cells was random, and there was no obvious alignment of the cells (Fig. S5<sup>†</sup>). As for the homogeneous microfibers, the cells grown on them were partly aligned: 78.09% of cells were elongated within  $30^{\circ}$  to the long axis of the fiber and 29.41% of cells were within  $10^{\circ}$  (Fig. 5E). On the heterogeneous microfibers, the cells were totally aligned: 98.13% of cells were

elongated within  $30^{\circ}$  to the long axis of the fiber and 65.51% of cells were within  $10^{\circ}$  (Fig. 5E). Furthermore, the results also revealed that the C2C12 cells exhibited the longest morphology on heterogeneous microfibers, which was also attributed to the confinement of cells in the grooves. These results showed that heterogeneous microfibers had a more significant effect on the maturity of C2C12 cells, indicating the potential of these grooved microfibers in the application of tissue engineering and regenerative medicine.

## 4. Conclusions

In summary, we propose a new strategy for the controlled spinning of grooved microfibers for engineering skeletal muscles. The grooved microfibers are formed based on a multifluid laminar flow design of the microfluidic device and NaA with various concentrations. The size and shape of the microfibers and the grooves can be easily controlled by adjusting the flow rates of NaA and CaCl<sub>2</sub>. By adding complex hydrogel prepolymers, the heterogeneous microfibers can be well-tailored due to the inherent properties of ionic crosslinking and photopolymerization. Moreover, the utility of the heterogeneous microfibers is successfully demonstrated by their ability to serve as anisotropic scaffolds for the cell directional alignment. The established system provides a flexible and controllable anisotropic scaffold for skeletal muscle engineering. The properties such as composition, configuration, and biocompatibility of the microfibers reveal the huge potential of the proposed method in multifunctional materials and regenerative medicine.

## Conflicts of interest

There are no conflicts of interest to declare.

## Acknowledgements

This research was supported by the Strategic Priority Research Program of the Chinese Academy of Sciences (Grant Nos. XDA16020900, XDB29050301, XDB32030200), the National Key R&D Program of China (No. 2017YFB0405404), the National Natural Science Foundation of China (Nos. 31971373, 81803492), the Yunnan Key Research and Development Program (No. 202003AD150009), the China Postdoctoral Science Foundation (No. 2019M660065), and the Innovation Program of Science and Research from the DICP, CAS (DICP I201934).

## References

- 1 M. Zhou, J. Gong and J. Ma, *e-Polym.*, 2019, **19**, 215–224.
- 2 E. Kim, M. Takeuchi, A. Hasegawa, A. Ichikawa, Y. Hasegawa, Q. Huang and T. Fukuda, *IEEE ASME Trans. Mechatron.*, 2020, **25**, 477–486.
- 3 S. Liang, Y. Tu, Q. Chen, W. Jia, W. Wang and L. Zhang, *Mater. Horiz.*, 2019, **6**, 2135–2142.
- 4 Y. Ni, W. Lin, R.-J. Mu, C. Wu, L. Wang, D. Wu, S. Chen and J. Pang, *RSC Adv.*, 2018, **8**, 26432–26439.
- 5 X. Deng, Y. Ren, L. Hou, W. Liu, T. Jiang and H. Jiang, *Small*, 2019, **15**, 1903098.
- 6 S. Nakajima, R. Kawano and H. Onoe, *Soft Matter*, 2017, **13**, 3710–3719.
- 7 Y. Tian, P. Zhu, X. Tang, C. Zhou, J. Wang, T. Kong, M. Xu and L. Wang, *Nat. Commun.*, 2017, **8**, 1–9.
- 8 R. Liu, B. Kong, Y. Chen, X. Liu and S. Mi, *Sens. Actuators, B*, 2020, **304**, 127069.
- 9 D. Kai, M. P. Prabhakaran, G. Jin and S. Ramakrishna, *J. Biomed. Mater. Res., Part B*, 2011, **98**, 379–386.
- 10 M. F. Daud, K. C. Pawar, F. Claeysens, A. J. Ryan and J. W. Haycock, *Biomaterials*, 2012, **33**, 5901–5913.
- 11 X. Wang, B. Ding and B. Li, *Mater. Today*, 2013, **16**, 229–241.
- 12 R. D. Pedde, B. Mirani, A. Navaei, T. Styan, S. Wong, M. Mehrali, A. Thakur, N. K. Mohtaram, A. Bayati, A. Dolatshahi-Pirouz, M. Nikkhah, S. M. Willerth and M. Akbari, *Adv. Mater.*, 2017, **29**, 1606061.
- 13 M. Costantini, C. Colosi, W. Swieszkowski and A. Barbetta, *Biofabrication*, 2018, **11**, 012001.
- 14 S. A. Bradner, M. McGill, A. Golding, R. Grudt and D. L. Kaplan, *Macromol. Mater. Eng.*, 2019, **304**, 1900045.
- 15 J. D. Liu, X. Y. Du, L. W. Hao, Q. Li and S. Chen, *ACS Appl. Mater. Interfaces*, 2020, **12**, 50823–50833.
- 16 Y. Yu, H. Wen, J. Ma, S. Lykkemark, H. Xu and J. Qin, *Adv. Mater.*, 2014, **26**, 2494–2499.
- 17 D. H. Yoon, K. Kobayashi, D. Tanaka, T. Sekiguchi and S. Shoji, *Lab Chip*, 2017, **17**, 1481–1486.
- 18 R. Xie, P. Xu, Y. Liu, L. Li, G. Luo, M. Ding and Q. Liang, *Adv. Mater.*, 2018, **30**, e1705082.
- 19 Y. Cheng, X. Zhang, Y. Cao, C. Tian, Y. Li, M. Wang, Y. Zhao and G. Zhao, *Appl. Mater. Today*, 2018, **13**, 116–125.
- 20 K. Maeda, H. Onoe, M. Takinoue and S. Takeuchi, *Adv. Mater.*, 2012, **24**, 1340–1346.
- 21 M. Nie and S. Takeuchi, *Sens. Actuators, B*, 2017, **246**, 358–362.
- 22 Z. Liu, C. Liu, Y. Zhang, Y. Zhang, X. Yang, J. Zhang, J. Yang and L. Yuan, *IEEE Photonics Technol. Lett.*, 2017, **29**, 2087–2090.
- 23 R. Yuan, J. Lee, H.-W. Su, E. Levy, T. Khudiyev, J. Voldman and Y. Fink, *Proc. Natl. Acad. Sci. U. S. A.*, 2018, **115**, E10830–E10838.
- 24 H. Liu, Y. Wang, W. Chen, Y. Yu, L. Jiang and J. Qin, *Mater. Sci. Eng., C*, 2019, **104**, 109705.
- 25 A. Kobayashi, K. Yamakoshi, Y. Yajima, R. Utoh, M. Yamada and M. Seki, *J. Biosci. Bioeng.*, 2013, **116**, 761–767.
- 26 E. Kang, G. S. Jeong, Y. Y. Choi, K. H. Lee, A. Khademhosseini and S. H. Lee, *Nat. Mater.*, 2011, **10**, 877–883.
- 27 Y. Cheng, Y. Yu, F. Fu, J. Wang, L. Shang, Z. Gu and Y. Zhao, *ACS Appl. Mater. Interfaces*, 2016, **8**, 1080–1086.
- 28 Y. Yu, W. Wei, Y. Wang, C. Xu, Y. Guo and J. Qin, *Adv. Mater.*, 2016, **28**, 6649–6655.
- 29 C. M. Hwang, Y. Park, J. Y. Park, K. Lee, K. Sun, A. Khademhosseini and S. H. Lee, *Biomed. Microdevices*, 2009, **11**, 739–746.
- 30 Y. Yang, X. Liu, D. Wei, M. Zhong, J. Sun, L. Guo, H. Fan and X. Zhang, *Biofabrication*, 2017, **9**, 045009.
- 31 Y. Yang, J. Sun, X. Liu, Z. Guo, Y. He, D. Wei, M. Zhong, L. Guo, H. Fan and X. Zhang, *Regener. Biomater.*, 2017, **4**, 299–307.

- 32 V. Hosseini, P. Kollmannsberger, S. Ahadian, S. Ostrovidov, H. Kaji, V. Vogel and A. Khademhosseini, *Small*, 2014, **10**, 4851–4857.
- 33 M. Ebrahimi, S. Ostrovidov, S. Salehi, S. B. Kim, H. Bae and A. Khademhosseini, *J. Tissue Eng. Regener. Med.*, 2018, **12**, 2151–2163.
- 34 X. Shi, S. Ostrovidov, Y. Zhao, X. Liang, M. Kasuya, K. Kurihara, K. Nakajima, H. Bae, H. Wu and A. Khademhosseini, *Adv. Funct. Mater.*, 2015, **25**, 2250–2259.
- 35 G. S. Jeong and S.-H. Lee, *Tissue Eng. Regener. Med.*, 2014, **11**, 291–296.
- 36 H. Wang, H. Liu, H. Liu, W. Su, W. Chen and J. Qin, *Adv. Mater. Technol.*, 2019, **4**, 1800632.
- 37 H. T. Liu, H. Wang, W. B. Wei, H. Liu, L. Jiang and J. H. Qin, *Small*, 2018, **14**, e1801095.
- 38 I. Braccini and S. Perez, *Biomacromolecules*, 2001, **2**, 1089–1096.
- 39 F. G. Donnan and R. C. Rose, *Can. J. Res., Sect. B*, 1950, **28**, 105–113.
- 40 H. Storz, U. Zimmermann, H. Zimmermann and W.-M. Kulicke, *Rheol. Acta*, 2009, **49**, 155–167.
- 41 M. G. Jensen, J. C. Knudsen, N. Viereck, M. Kristensen and A. Astrup, *Food Chem.*, 2012, **132**, 823–829.
- 42 M. Bogun, *Fibres Text. East. Eur.*, 2009, **17**, 17–22.
- 43 N. Aoyama, I. Hayakawa, N. Akiba and S. Minakuchi, *Prosthodont. Res. Pract.*, 2007, **6**, 239–245.
- 44 J. Shao, L. Wu, J. Wu, Y. Zheng, H. Zhao, Q. Jin and J. Zhao, *Lab Chip*, 2009, **9**, 3118.
- 45 T. D. Usal, D. Yucel and V. Hasirci, *Int. J. Biol. Macromol.*, 2019, **121**, 699–706.
- 46 Y. Gao and X. Jin, *Mar. Drugs*, 2019, **17**, 557.
- 47 C. Colosi, S. R. Shin, V. Manoharan, S. Massa, M. Costantini, A. Barbetta, M. R. Dokmeci, M. Dentini and A. Khademhosseini, *Adv. Mater.*, 2016, **28**, 677–684.
- 48 J. W. Nichol, S. T. Koshy, H. Bae, C. M. Hwang, S. Yamanlar and A. Khademhosseini, *Biomaterials*, 2010, **31**, 5536–5544.
- 49 K. Yue, G. Trujillo-de Santiago, M. M. Alvarez, A. Tamayol, N. Annabi and A. Khademhosseini, *Biomaterials*, 2015, **73**, 254–271.
- 50 J. Kim, J. Leem, H. N. Kim, P. Kang, J. Choi, M. F. Haque, D. Kang and S. Nam, *Microsyst. Nanoeng.*, 2019, **5**, 1–10.